Compressing magnetic fields with high-energy lasers[a)]

J. P. Knauer,[1,b)] O. V. Gotchev,[1,2,3] P. Y. Chang,[1,4] D. D. Meyerhofer,[1,2,3,4] O. Polomarov,[2,3]
R. Betti,[1,2,3,4] J. A. Frenje,[2,5] C. K. Li,[2,5] M. J.-E. Manuel,[2,5] R. D. Petrasso,[2,5]
J. R. Rygg,[6] and F. H. Séguin[2,5]

[1]*Laboratory for Laser Energetics, University of Rochester, 250 East River Road,
Rochester, New York 14623, USA*
[2]*Fusion Science Center for Extreme States of Matter and Fast Ignition Physics, University of Rochester,
250 East River Road, Rochester, New York 14623, USA*
[3]*Department of Mechanical Engineering, University of Rochester, 250 East River Road,
Rochester, New York 14623, USA*
[4]*Department of Physics and Astronomy, University of Rochester, 250 East River Road,
Rochester, New York 14623, USA*
[5]*Plasma Science and Fusion Center, MIT, Cambridge, Massachusetts 02139, USA*
[6]*Lawrence Livermore National Laboratory, Livermore, California 94550, USA*

Laser-driven magnetic-field compression producing a magnetic field of tens of megaGauss is reported for the first time. A shock wave formed during the implosion of a cylindrical target traps an initial (seed) magnetic field that is amplified via conservation of magnetic flux. Such large fields are expected to magnetize the electrons in the hot, central plasma, leading to a cyclotron frequency exceeding the collision frequency. The Omega Laser Facility [T. R. Boehly *et al.*, Opt. Commun. **133**, 495 (1997)] was used to implode cylindrical CH targets filled with deuterium gas and seeded with an external field ($>$50 kG) from a magnetic pulse generator. This seed field is trapped and rapidly compressed by the imploding shell, minimizing the effect of resistive flux diffusion. The compressed field was probed via proton deflectrometry using 14.7 MeV protons from the D+^{3}He fusion reaction emitted by an imploding glass microballoon. Line-averaged magnetic fields of the imploded core were measured to between 30 and 40 MG. Experimental data were analyzed with both a magnetohydrodynamic version of the one-dimensional hydrocode *LILAC* [J. Delettrez *et al.*, Phys. Rev. A **36**, 3926 (1987); N. W. Jang *et al.*, Bull. Am. Phys. Soc. **51**, 144 (2006)] and the particle propagation code GEANT4 [S. Agostinelli *et al.*, Nucl. Instrum. Methods Phys. Res. A **506**, 250 (2003)]. © *2010 American Institute of Physics*. [doi:10.1063/1.3416557]

I. INTRODUCTION

Laser-driven inertial confinement fusion (ICF) has seen significant progress in recent years for both direct[1,2] and indirect drive.[3] The energy E_{TN} released from an ICF implosion that has reached ignition conditions depends on the assembled fuel mass. The energy gain G is defined as E_{TN}/E_L, and for direct-drive implosions, it can be shown[4] that the gain of a target that has ignited scales as $G \sim V_i^{-1.25} I_L^{-0.29}$, where V_i is the implosion velocity and I_L is the laser intensity. The thermonuclear gain is therefore roughly inversely proportional to the implosion velocity. In conventional ICF, successful ignition of the assembled central hot spot requires that the hot spot reach certain temperature T_{hs} (of the order of 5 keV ion temperature). Scaling relations[4] for direct-drive ICF show that $T_{hs} \sim V_i^{1.4}$. If the compression has too low a velocity, it cannot overcome thermal losses and the hot spot will not reach the required temperature, although the areal density of the fuel may attain high values. This restriction on V_i limits the minimum energy for ignition.

In a magnetoinertial fusion implosion, additional thermal insulation of the fuel forming the hot spot is provided by a strong magnetic field in an otherwise typical direct-drive ICF

target.[5] This differs from magnetized target fusion,[6–9] which occupies an intermediate region of parametric space, closer to magnetic confinement fusion. Provided that the magnetic field is sufficiently strong, the benefits of this approach are twofold: The hot spot can reach ignition temperatures because of the reduced electron thermal conductivity. When the nuclear burn develops, the alpha particles can be confined, by a strong magnetic field, to the burn region delivering the energy where it is needed to support the burn wave. Considering a characteristic 40 μm hot-spot radius and requiring electron and alpha-particle gyroradii be smaller than this sets the required magnetic fields at $B > 100$ kG for 30 keV electrons and $B > 95$ MG for the 3.5 MeV fusion alphas in a burning Deuterium-Tritium (DT) plasma. Such strong magnetic fields are difficult to create externally. The largest macroscopic magnetic fields have so far been generated only by magnetic flux compression in metallic liners driven by chemical detonation[10] and pulsed-power generators.[11] Strong magnetic fields have also been measured and inferred from Z-pinch gas puff experiments on pulsed-power generators.[11] Flux compression with an ICF-scale laser like OMEGA is a path to even stronger fields. The idea is to perform an ICF implosion in which there is a preimposed macroscopic magnetic field, trapped in the converging target plasma. Flux compression with a plasma "liner" was discussed by Liber-
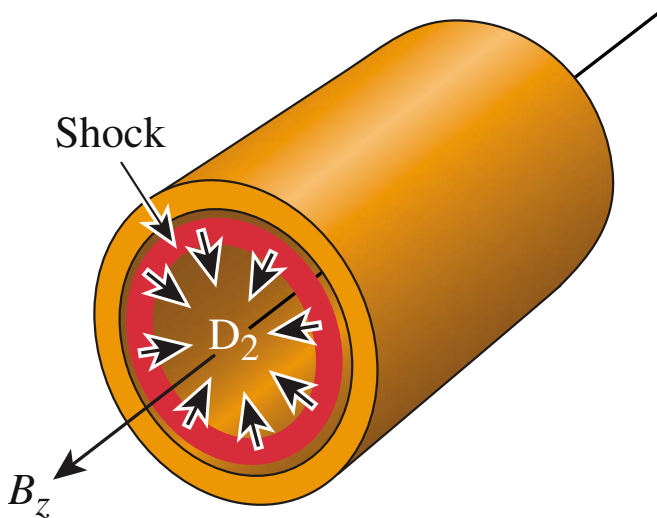
FIG. 1. (Color online) Schematic of how a laser-driven liner traps a seed magnetic field and compresses it. The initial laser pulse generates a shock wave that breaks out of the shell into the interior gas. The gas is then ionized, creating a conductive shell that traps the seed field. Kinetic energy given to the shell then compresses the field and amplifies it.
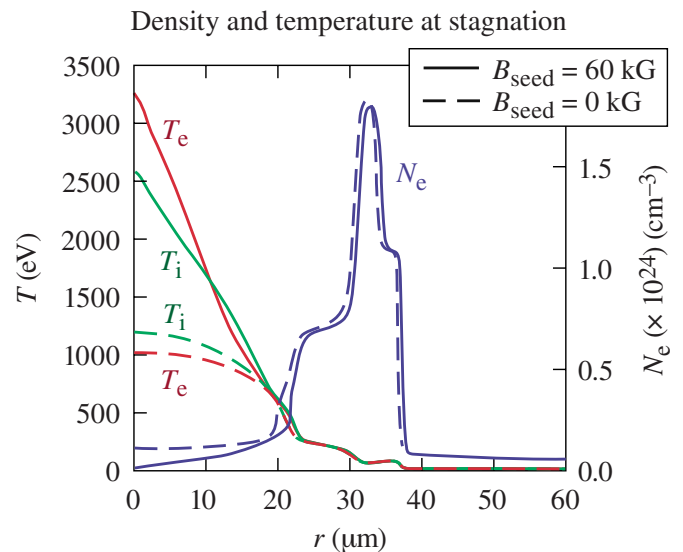

FIG. 2. (Color online) The temperature and density profiles at the center of the target, as simulated by LILAC MHD for the time of peak compression for initial seed field values of 0 (dashed lines) and 60 kG (solid lines).

man and Velikovich in Refs. [12] and [13] more than 20 years ago. In Ref. [13], the authors consider a magnetic field that is "frozen in" plasma compressed by a thin cylindrical wall. They show effective compression of the field with low diffusion losses.

This research is concerned with the compression of magnetic flux, initially axial in cylindrical geometry by high-beta plasmas under ICF conditions. The magnetic pressure is a small perturbation to the hydrodynamic pressure in these laser plasmas.

Section II discusses the concept of magnetic-flux compression. OMEGA experiments are detailed in Sec. III. Analysis of the experimental data is presented in Sec. IV. A summary and future work are discussed in Sec. V.

II. MAGNETIC-FLUX COMPRESSION

In cylindrical geometry, if the diffusion of the magnetic field is neglected, the conservation of the magnetic flux Φ requires that the magnetic field increases in proportion to the reduction in the encircled area

$$B_{\max} = B_0 \left(\frac{Re_0}{Re_{\min}} \right)^2. \tag{1}$$

When the diffusion of flux into the plasma shell due to its finite resistivity is considered, Eq. (1) is modified to

$$B_{\max} = B_0 \left(\frac{Re_0}{Re_{\min}} \right)^{2(1-1/Re_m)}, \tag{2}$$

where Re_m is an appropriate time-averaged value of the magnetic Reynolds number. Re_m can be defined as the ratio of the magnetic field's convective diffusion time $\tau_{\text{diffusion}}$ to the flux compression time $\tau_{\text{implosion}}$.

An ICF-scale, cylindrical-ablator shell (usually plastic) driven by a laser does not, by itself, trap the enclosed magnetic flux in contrast to compression with metallic liners.

This is shown schematically in Fig. 1. At the onset of the laser pulse with a peak intensity of 5×10^{14} W/cm², the rapid increase in ablation pressure drives a shock wave through the shell; it breaks out into the gas that fills the capsule, raising the temperature in the postshock region to about 100 eV and fully ionizing the gas behind the shock wave. The diffusion time $\tau_{\text{diffusion}}$ is given by $4\pi\sigma\delta^2/c^2$, where σ is the conductivity behind the shock and δ is the thickness of the shocked gas; $\tau_{\text{diffusion}}$ is ~200 ns. The colder and more resistive shell then provides the mechanical work for compression of this plasma and the field embedded in it. The implosion time $\tau_{\text{implosion}}$ is given by the shell radius divided by the implosion velocity V_i; $\tau_{\text{implosion}}$ is ~4 ns for the OMEGA cylindrical implosions. A time-averaged value of $Re_m > 50$ is obtained for these values of $\tau_{\text{diffusion}}$ and $\tau_{\text{implosion}}$. The temperature and density profiles at the center of the target, as simulated by the *LILAC* magnetohydrodynamic (MHD) code, are shown in Fig. 2 for the time of peak compression for initial seed field values of 0 and 60 kG. These were runs for a 1.5 mm long, cylindrical plastic shell with 860 μm diameter and 20 μm thickness that was filled with 3 atm of D₂. In the hot spot (in this case the central 20 μm of the target), both the electron and ion temperatures were larger when the seed field was present. The magnetic field had little effect on the shell's density but the central density was reduced with a magnetic field because of the higher temperatures and magnetic pressure for an isobaric implosion.

III. OMEGA EXPERIMENT

The OMEGA laser[14] is an ideal test bed for magnetic-flux compression experiments. Typical implosion velocities V_i in excess of 10^7 cm/s, coupled with the high conductivity of the hot, dense plasma containing the field, provide effective compression of the seed magnetic flux with low diffusion losses. Multi-megaGauss compressed fields are due to
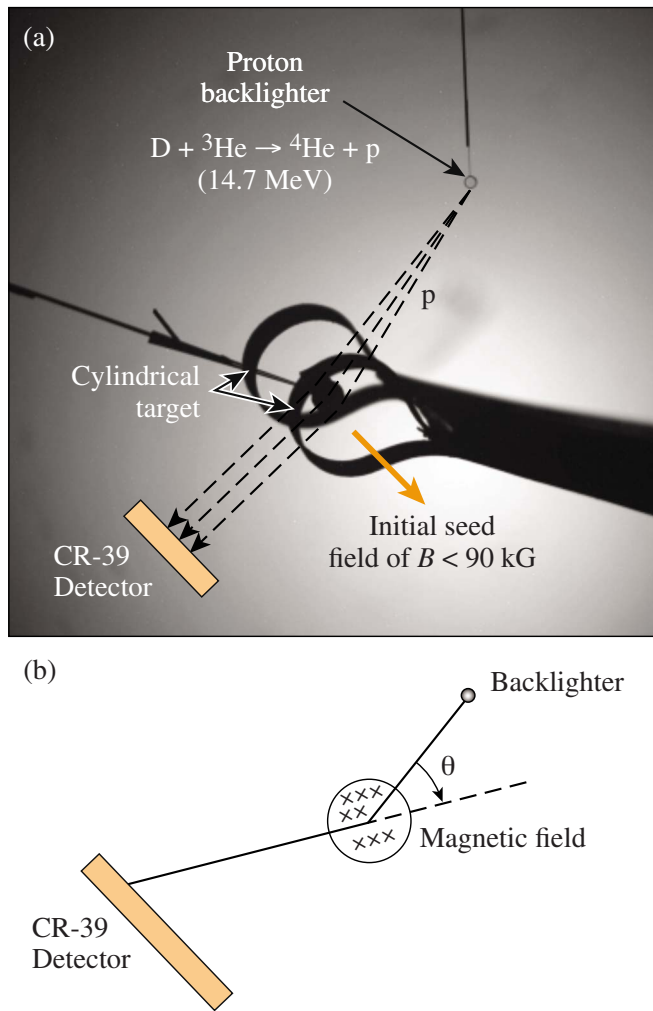
FIG. 3. (Color online) (a) An image of the magnetic-field generator's coils, the cylindrical target between the coils, and the proton backlighter target. The initial seed field is less than 90 kG in the region of the cylindrical target and varies by no more than 5% over the volume of the cylinder. The proton backlighter is a glass microballoon filled with a D ^{3}He gas mixture that is the source of the protons detected by CR-39 foils. (b) A schematic showing the geometry used to measure the magnetic field by proton deflection. The proton trajectory from the backlighter is shown as a solid line. The deflection angle (θ) is defined as the angle between the final trajectory and the initial trajectory.

the convergence of laser-driven implosions. A compact device generating seed magnetic fields of sufficient strength (up to 0.15 MG measured) was built to test the laser-driven magnetic-flux compression concept.[15] It fits in a diagnostic insertion vacuum interlock on the OMEGA chamber, stores less than 150 J, and provides magnetic pulses with intensities of 0.05–0.15 MG and ~400 ns duration.

Figure 3 is an image of the experimental configuration at the center of the OMEGA target chamber and a schematic of the magnetic-field measurement geometry. There are four components that compress and then measure the magnetic field shown in Fig. 3(a). The field generator and the cylindrical target are placed at the center of the target chamber, and a backlighter target is placed 9 mm from the target chamber center opposite a detector that uses aluminum and CR-39 foils, located 105 mm from the center of the target chamber, to record the protons that pass through the imploded cylin-

der. Proton radiograph images recorded by the CR-39 of the cylindrical implosion have a 12.7× magnification. The schematic depicted by Fig. 3(b) shows an axial view of a planar cross-section of the proton backlighter technique used to measure the magnetic field. Proton paths from the backlighter target to the CR-39 recorder are perpendicular to the axial field. Protons are deflected by the magnetic field with the deflection angle defined as the angle between the final trajectory (solid line) and the initial proton trajectory.

The magnetic flux was compressed inside an imploded 1.5 mm-long CH cylinder filled with 3 atm of D_2 gas. This cylinder had an initial diameter of 860 μm and a wall thickness of 20 μm. This is the same target used to simulate the implosion of a magnetized target and shown in Fig. 2. Two large end caps were glued onto the ends of the cylinder, the outside surface of which was coated with a 1000 Å layer of aluminum to retain the gas. It was found that a fill tube connected to a gas reservoir was necessary to keep the D_2 at the initial pressure. The implosion target was then inserted on the axis midway between the coils used to generate the seed magnetic field. Coils of 4 mm diameter and separated by 5.15 mm optimized the laser illumination on the cylinder and the field uniformity in the region of the cylinder.

A monoenergetic ($\Delta E/E \sim 0.03$), pointlike (size/object distance ~0.01), time-gated (~150 ps burst) proton source was provided by the implosion of a glass sphere filled with a D ^{3}He gas mixture. The 14.7 MeV protons produced by the D–^{3}He fusion reactions were accelerated to ~15.2 MeV by charging the backlighter target, creating an electric field.[16] These glass spheres were 400 μm in diameter with wall thicknesses between 2.1 and 2.4 μm and filled to a pressure of 10 atm. These targets were the same as those used for previous proton backlighter measurements.[17–19]

The 60-beam OMEGA laser was configured so that 40 beams were used to implode the cylinder (drive beams) and 20 beams (backlighter beams) were used to implode the glass sphere. The laser pulse shape for the drive beams and backlighter beams was a 1 ns wide square pulse. The drive beams were configured with SG4 distributed phase plates (DPPs),[20] polarization smoothing,[21] and full-bandwidth smoothing by spectral dispersion.[22] These 40 beams were pointed to minimize the illumination nonuniformity at the surface of the cylinder. The laser energy incident on the cylindrical target was 14 kJ, giving an intensity of 5×10^{14} W/cm^2. The backlighter beams used no DPPs and were focused onto the glass sphere with a spot diameter of 300 μm. A proton backlighter target yield of 3×10^7 gave a proton flux of 0.3 protons per μm^2 at the target and 20 000 protons per cm^2 at the detector.

IV. RESULTS

The compressed fields within the dense, optically thick ICF plasmas are difficult to measure. Figure 4 shows how proton deflectometry based on the method described in Refs. 17–19 is used on OMEGA to measure the magnetic field after compression. In Fig. 4(a), the strong magnetic field is restricted to the hot spot with the dense shell containing a much smaller residual field. Protons from the backlighter are deflected into two peaks. The first peak, nearest
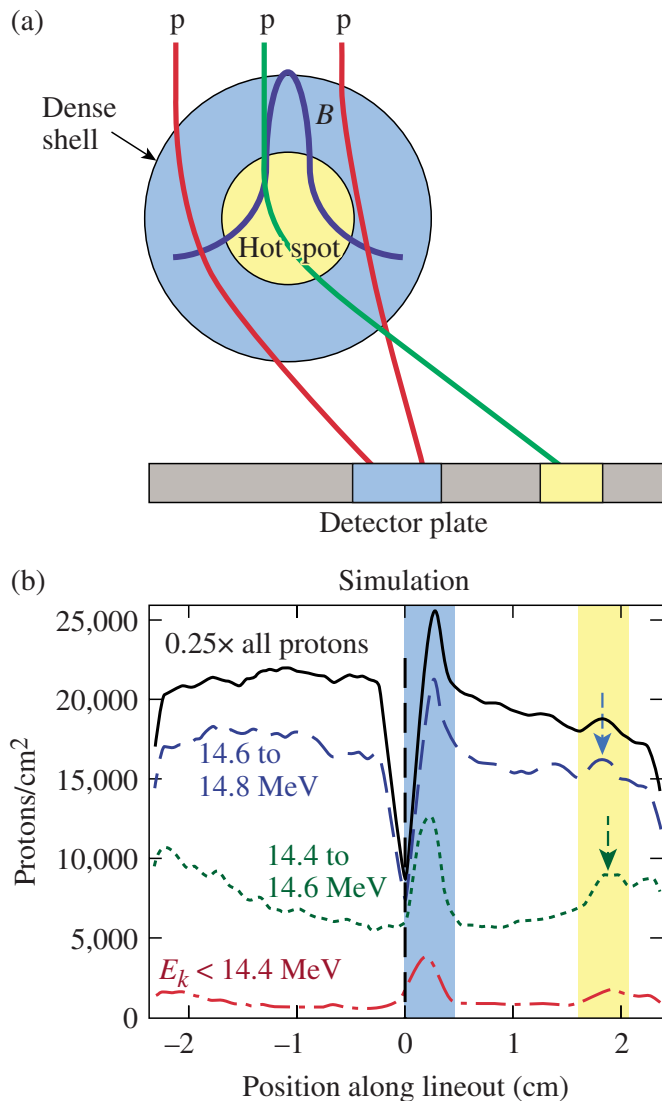
(a)

(b) Simulation

FIG. 4. (Color online) (a) An image of the propagation of protons through the imploded cylindrical target and detected by CR-39. There is a low-density hot spot surrounded by a high-density shell. The compressed magnetic field peaks in the center of the hot spot and has a tail that extends into the shell. (b) The result of a GEANT4 calculation revealing the presence of two deflection peaks in the proton radiograph.

the center of the image, is created when protons propagating through the shell but missing the hot spot are bent by the residual field in the dense shell. A second peak, farthest from the center, is formed by the protons that traverse the hot spot and encounter the strong magnetic field. Protons that propagate only through the shell have less deflection but lose more energy. A discrimination of tracks by energy (track diameter) was implemented to separate the hot spot (strong field)—traversing protons from the background "free-space" particles that land in the same area of the detector. This is shown in Fig. 4(b) as a plot of track density versus position for all protons (solid curve), protons with an energy greater than 14.6 MeV but less than 14.8 MeV (dashed curve), protons with energies between 14.4 and 14.6 MeV (dotted curve), and protons with an energy less than 14.4 MeV (dot-dashed curve). These data came from a calculation to simulate the deflected protons.

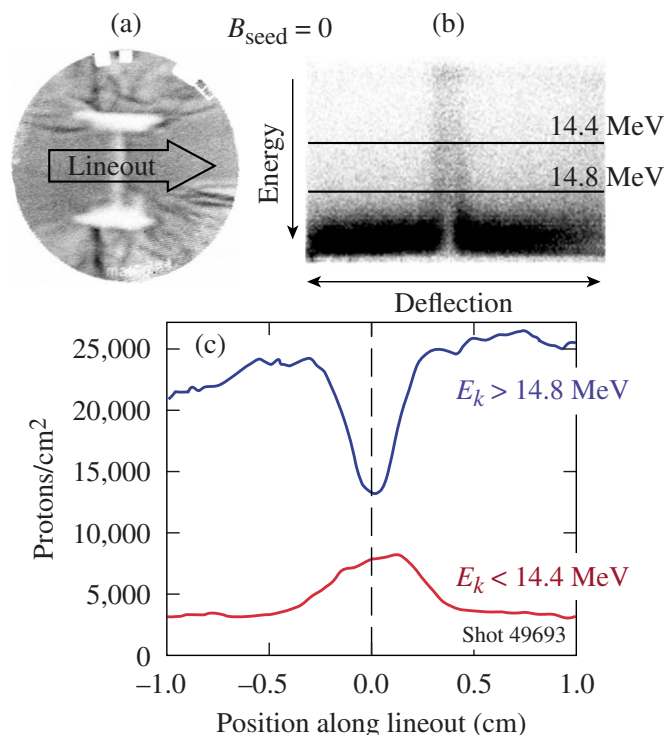(a) $B_{seed} = 0$ (b)

(c)

FIG. 5. (Color online) Data from a cylindrical implosion with no magnetic field. (a) An image of the proton track density recorded by a piece of CR-39. Proton tracks were analyzed along a linear region shown by the "Lineout" arrow perpendicular to the axis of the implosion. (b) A scatter plot of the track diameter vs the deflection (or position along the CR-39 foil). The track diameter is proportional to the track energy with higher energy protons having smaller diameter tracks. Therefore, protons with low energies are at the top of image (b) and higher energy protons are at the bottom of image (b). (c) A plot of two lineouts taken through the scatter plot corresponding to protons with energies <14.4 and <14.8 MeV. There is no evidence of protons being deflected from their original paths.

Experimental verification of the deflectometry technique is shown in Fig. 5 (seed field=0) and Fig. 6 (seed field=56 kG). Figure 5(a) shows an image of the CR-39 track detector; these data are plotted as a scatter plot of track diameter versus track position in Fig. 5(b). Figure 5(b) was used to construct the lineouts shown in Fig. 5(c) by taking a band of data and averaging over its width. The upper curve in Fig. 5(c) is from tracks with energy $E_k < 14.8$ MeV; the lower curve is from tracks with $E_k < 14.4$ MeV caused by an additional slowing down through the compressed target. This plot shows a symmetrical peak in the proton density consistent with no deflection in the target field. In contrast, the same type of data shown in Fig. 6, for a case where there was a seed field, shows an asymmetric peak attributable to the deflection of the magnetic field. The lower plot in Fig. 6(c) shows protons that have lost energy propagating through the compressed target and not the background protons.

A simulation package based on the Monte Carlo particle-transport framework GEANT4 (Ref. 23) was developed to predict and interpret the experimental data. After including the field topology and material parameters predicted by the *LILAC* MHD code[24,25] for the time of proton probing, the particle-transport code computes the deflection pattern under the combined action of the field and scattering/energy loss processes. A comparison (Fig. 7) of the experimental data (a)
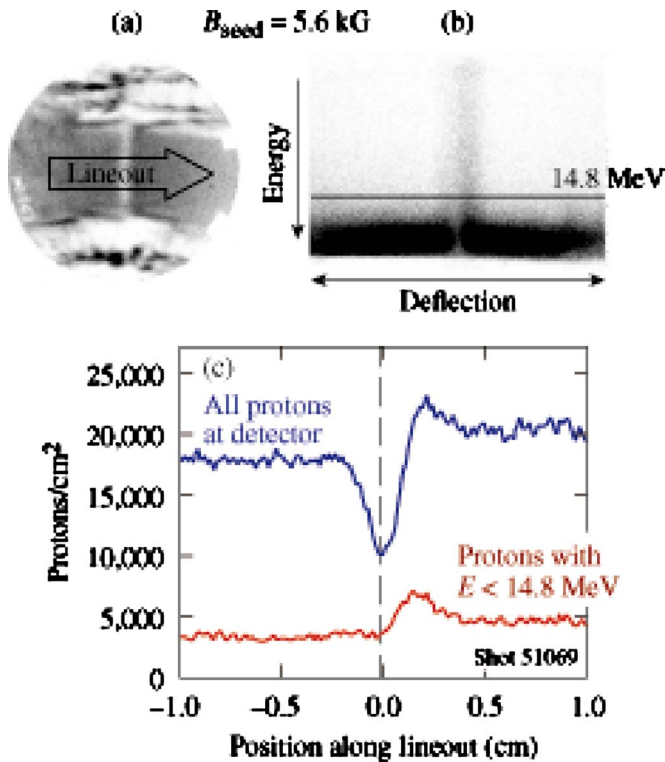
FIG. 6. (Color online) Data from a cylindrical implosion with a seed magnetic field of 5.6 kG. (a) An image of the proton track density recorded by a piece of CR-39. Proton tracks were analyzed along a linear region shown by the Lineout arrow perpendicular to the axis of the implosion. (b) A scatter plot of the track diameter vs the deflection (or position along the CR-39 foil). The track diameter is proportional to the track energy with higher energy protons having smaller diameter tracks. Therefore, protons with low energies are at the top of image (b) and higher energy protons are at the bottom of image (b). (c) A plot of two lineouts taken through the scatter plot corresponding to a sum of all protons and protons with energies <14.8 MeV. There is evidence of protons being deflected by the magnetic field in the shell.

and simulation predictions (b) for shot 51 069, which had a 56 kG seed field, shows good qualitative agreement, capturing the double-peak deflection pattern. The protons that were slowed down the most (bottom curve) were those that crossed through the shell but not the hot spot, missing the peak field. From the peak deflection of 1.8 ± 0.1 cm (marked with an arrow), one can estimate an average product $\langle R_{hs} B_{max} \rangle \approx 2(\theta)(m_p v_p / e)c$ or 0.052 MG cm, corresponding to a 30 MG hot-spot field for a predicted hot-spot radius of 17 μm. The deflection of the first peak can be used to estimate a residual magnetic field in the shell of 0.8 MG averaged over the shell thickness. The error in the magnetic field measurement comes from two sources: the error in the deflection (0.1 cm) and the error in the hot-spot radius. The statistical error of the hot-spot radius can be estimated by looking at the total number of measured protons that pass through the core and shell, which is constrained by the GEANT4 fit to the data. A 0.5 mm section of a 17 μm radius core will have ~400 protons in the peak with the largest deflection resulting in an error of 5% for the core size. The measured magnetic field is 30 ± 2 MG. The shell is estimated to be 70 μm in diameter, and the first peak (smallest deflection) will have ~1300 protons in a 0.5-mm-wide
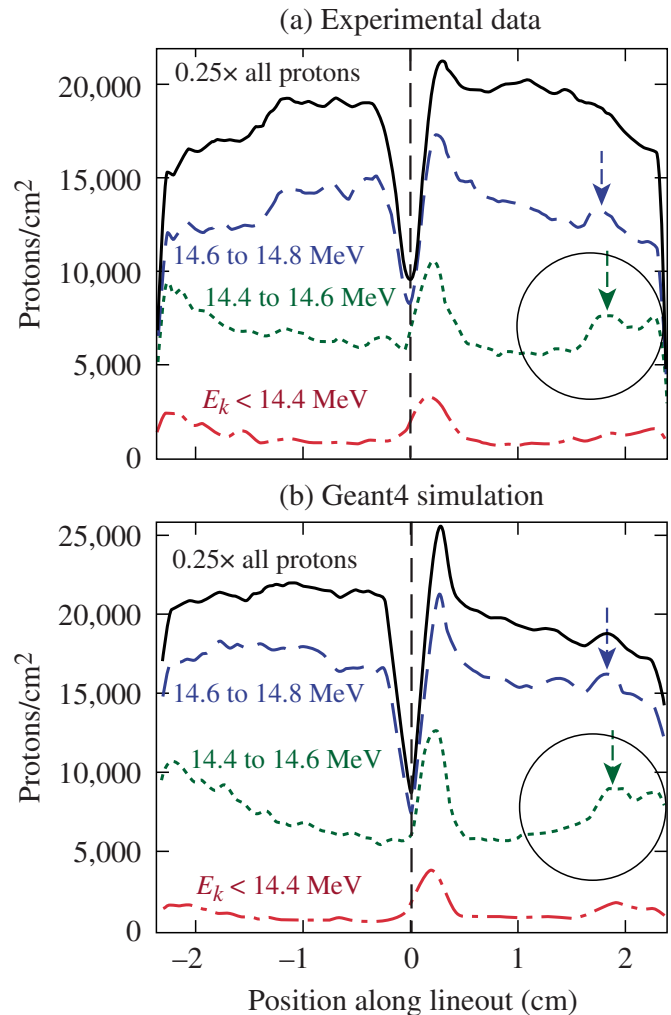

FIG. 7. (Color online) Plots of the proton track position for all protons and for protons in three energy bands. (a) The experimental data indicating a deflection peak at 1.9 cm from the core center reference. (b) The GEANT4 calculation using hydrodynamic simulation data to calculate the proton spectrum and track position. There is excellent agreement between the experimental plots and the GEANT4 plots.

lineout for an error of 3% in the shell size. The magnetic field in the shell is 0.8 ± 0.1 MG.

When the seed field's direction was reversed (via reversal of the current in the coils), the deflection pattern (Fig. 8, shot 52 532) reversed direction. This confirms the magnetic nature of the deflection and supports the "relocation" of the high-field deflection to the other side of the core. This is evident in lineouts at several energies shown in Fig. 8, where in addition to the offset peak near the center, there is again a concentration of tracks away from it (at -2.0 cm), caused by the peak of the compressed field in the hot spot. Analysis of the peak deflection revealed that the higher seed field (-62 kG) for this shot was amplified to at least -36 ± 3 MG. The fields determined from Figs. 7(a) and 8 are the most conservative values, given by the lowest field B_{max}, spread over the largest radius R_{hs}, which can result in the observed deflection $\theta \sim \langle R_{hs} B_{max} \rangle$ without violating the flux conservation condition $\Phi \sim \langle R_{hs}^2 B_{max} \rangle \leq \Phi_0$. If the more realistic case is considered, where up to 40% of the initial magnetic flux ($\Phi_0 \approx 360$ G cm^2) is lost as predicted by the hydrodynamic
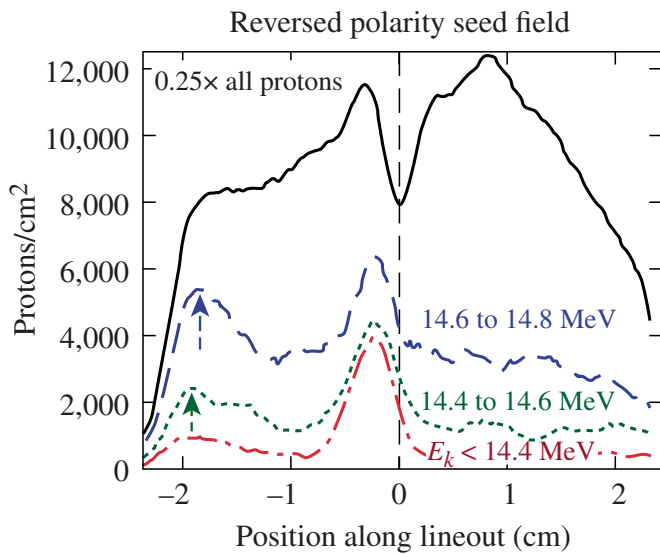
FIG. 8. (Color online) A plot of proton track position for all protons and for protons in three energy bands [similar to Fig. 7(a)]. The polarity of the seed magnetic field was reversed. The position of the deflection peaks is now on the opposite side of the core reference.

lisions of the 8 keV ions with thermal electrons and ions are $\Lambda_{ie} \approx 5$ and $\Lambda_{ii} \approx 8.6$, respectively. It is clear that the ions, having an ~ 6 μm mean free path, will undergo only a few collisions before leaving the hot spot. The electrons are fully magnetized but are thermally decoupled from the ions since the thermal equilibration time is of the order of 100 ps. As noted earlier, the higher temperatures are accompanied by lower hot-spot densities (Fig. 2) and lower plasma pressures since the total pressure (plasma+magnetic) is approximately independent of the magnetic field.

simulation, the estimated magnetic fields need to be revised upward to match the observed deflections.

The effect of the amplified magnetic field on the neutron yields was expected to be small for this experimental configuration even though the one-dimensional hydrocode predicts a two to three times increase in the yield caused by the temperature increase from thermal insulation in the hot spot. In the magnetized hot spot, the hydrocode did not correctly predict the fusion rate since the hot-spot size is such that the hot ions most likely to undergo fusion reactions (at the Gamow peak) are in the kinetic regime with their mean free path comparable to the hot-spot radius. For hot-spot conditions where $n_{e,hs} = 8 \times 10^{22}$ cm^{-3}, $T_{hs} = 1.5$ keV, the Gamow peak is at 8.2 keV, and the Coulomb logarithms for the col-
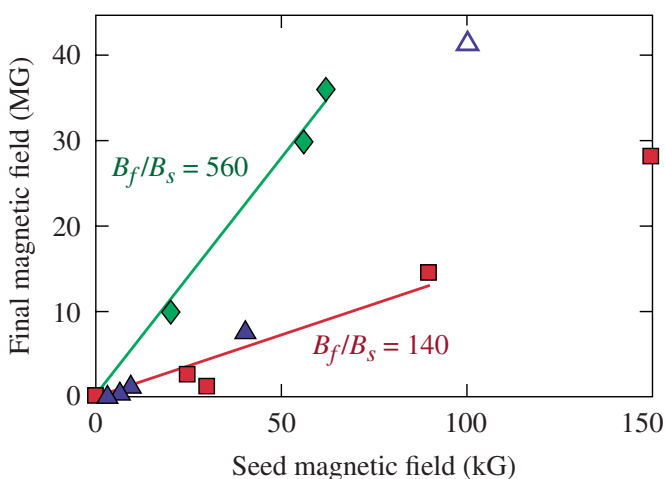

FIG. 9. (Color online) A plot of the final magnetic field vs the initial magnetic field for three different types of flux compression. The data shown by squares are from high-explosive-driven implosions. The triangles show data from electromagnetically driven implosions. Data for laser-driven implosions from this work are shown as diamonds.
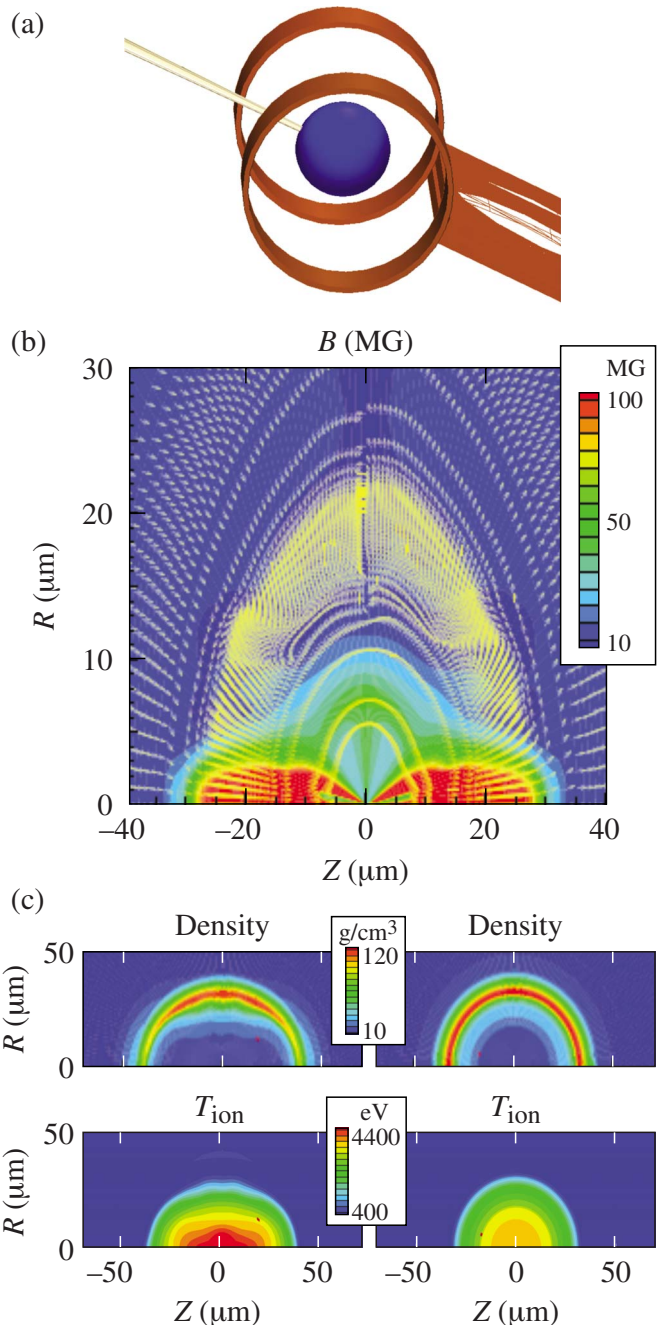

FIG. 10. (Color online) (a) Two-dimensional hydrodynamic simulations for a spherical target placed between the coils of the magnetic-field generator. (b) The magnetic field for the compressed spherical target. (c) The density and temperature distributions are shown with and without a magnetic field.

V. CONCLUSION

In summary, very high magnetic-flux compression has been achieved using the ablative pressure of the OMEGA laser to drive a cylindrical shell at high implosion velocity, trapping and compressing the embedded external field to 30 ± 2 and 36 ± 3 MG—high enough to magnetize the hot-spot center. These magnetic fields were measured using the deflection of protons emitted from a glass microballoon filled with D ^{3}He gas. Figure 9 is a plot of the compressed magnetic field as a function of the initial seed field for high-explosive (squares),[10] pulsed-power (triangles),[11] and laser-driven (diamonds) (this work) magnetic compression. The two lines are fits through the high-explosive and laser-driven data. The slope of the lines represents the amplification of the magnetic field caused by the implosion. An amplification factor of 140 seen in the high-explosive data represents a convergence (initial radius divided by the final radius) of 12. Laser-driven implosions have an amplification factor of 560, representing a convergence of 24.

Finding the parameter space where the target performance will be most affected by the compressed magnetic is the next step in these studies. The two-dimensional hydrodynamics code *DRACO* (Ref. 26) was modified to include resistive MHD and used to simulate the implosion of a spherical target inserted into the seed field created by the two coils [Fig. 10(a)]. The results are shown in Figs. 10(b) and 10(c). The magnetic-field structure of the imploded target is presented in Fig. 10(b), clearly showing the effect of the seed field. The compressed field peaks at about 100 MG at the center of the hot spot and shows an elongated hot spot attributable to the axial geometry of the initial magnetic field. Figure 10(c) shows the calculated density and temperatures for cases with and without a seed field. The seed field clearly increases the temperature of the hot spot and lowers the density with an initial magnetic field. Spherical targets will allow one to systematically study hot-spot conditions as a function of magnetic field.

ACKNOWLEDGMENTS

[1]S. E. Bodner, D. G. Colombant, J. H. Gardner, R. H. Lehmberg, S. P. Obenschain, L. Phillips, A. J. Schmitt, J. D. Sethian, R. L. McCrory, W. Seka, C. P. Verdon, J. P. Knauer, B. B. Afeyan, and H. T. Powell, Phys. Plasmas **5**, 1901 (1998).

[2]R. L. McCrory, D. D. Meyerhofer, S. J. Loucks, S. Skupsky, R. Betti, T. R. Boehly, T. J. B. Collins, R. S. Craxton, J. A. Delettrez, D. H. Edgell, R. Epstein, K. A. Fletcher, C. Freeman, J. A. Frenje, V. Yu. Glebov, V. N. Goncharov, D. R. Harding, I. V. Igumenshchev, R. L. Keck, J. D. Kilkenny, J. P. Knauer, C. K. Li, J. Marciante, A. Marozas, F. J. Marshall, A. V. Maximov, P. W. McKenty, S. F. B. Morse, J. Myatt, S. Padalino, R. D. Petrasso, P. B. Radha, S. P. Regan, T. C. Sangster, F. H. Séguin, W. Seka, V. A. Smalyuk, J. M. Soures, C. Stoeckl, B. Yaakobi, and J. D. Zuegel, J. de Phys. IV **133**, 59 (2006).

[3]The National Ignition Campaign Team and B. A. Hammel, Plasma Phys. Controlled Fusion **48**, B497 (2006).

[4]R. Betti and C. Zhou, Phys. Plasmas **12**, 110702 (2005).

[5]P. W. McKenty, V. N. Goncharov, R. P. J. Town, S. Skupsky, R. Betti, and R. L. McCrory, Phys. Plasmas **8**, 2315 (2001).

[6]I. R. Lindemuth, R. E. Reinovsky, R. E. Chrien, J. M. Christian, C. A. Ekdahl, J. H. Goforth, R. C. Haight, G. Idzorek, N. S. King, R. C. Kirkpatrick, R. E. Larson, G. L. Morgan, B. W. Olinger, H. Oona, P. T. Sheehey, J. S. Shlachter, R. C. Smith, L. R. Veeser, B. J. Warthen, S. M. Younger, V. K. Chernyshev, V. N. Mokhov, A. N. Demin, Y. N. Dolin, S. F. Garanin, V. A. Ivanov, V. P. Korchagin, O. D. Mikhailov, I. V. Morozov, S. V. Pak, E. S. Pavlovskii, N. Y. Seleznev, A. N. Skobelev, G. I. Volkov, and V. A. Yakubov, Phys. Rev. Lett. **75**, 1953 (1995).

[7]R. E. Siemon, I. R. Lindemuth, and K. F. Schoenberg, Comments Plasma Phys. Controlled Fusion **18**, 363 (1999).

[8]Y. C. F. Thio, E. Panarella, R. C. Kirkpatrick, C. E. Knapp, F. Wysocki, P. Parks, and G. Schmidt, in *Current Trends in International Fusion Research—Proceedings of the Second Symposium*, edited by E. Panarella (NRC Research, Ottawa, 1999), p. 113.

[9]D. D. Ryutov and Y. C. F. Thio, Fusion Sci. Technol. **49**, 39 (2006).

[10]A. D. Sakharov, Sov. Phys. Usp. **9**, 294 (1966).

[11]F. S. Felber, M. M. Malley, F. J. Wessel, M. K. Matzen, M. A. Palmer, R. B. Spielman, M. A. Liberman, and A. L. Velikovich, Phys. Fluids **31**, 2053 (1988).

[12]M. A. Liberman and A. L. Velikovich, J. Plasma Phys. **31**, 369 (1984).

[13]A. L. Velikovich, S. M. Gol'berg, M. A. Liberman, and F. S. Felber, Sov. Phys. JETP **61**, 261 (1985).

[14]T. R. Boehly, D. L. Brown, R. S. Craxton, R. L. Keck, J. P. Knauer, J. H. Kelly, T. J. Kessler, S. A. Kumpan, S. J. Loucks, S. A. Letzring, F. J. Marshall, R. L. McCrory, S. F. B. Morse, W. Seka, J. M. Soures, and C. P. Verdon, Opt. Commun. **133**, 495 (1997).

[15]O. V. Gotchev, J. P. Knauer, P. Y. Chang, N. W. Jang, M. J. Shoup III, D. D. Meyerhofer, and R. Betti, Rev. Sci. Instrum. **80**, 043504 (2009).

[16]D. G. Hicks, C. K. Li, F. H. Séguin, A. K. Ram, J. A. Frenje, R. D. Petrasso, J. M. Soures, V. Yu. Glebov, D. D. Meyerhofer, S. Roberts, C. Sorce, C. Stöckl, T. C. Sangster, and T. W. Phillips, Phys. Plasmas **7**, 5106 (2000).

[17]C. K. Li, F. H. Séguin, J. A. Frenje, J. R. Rygg, R. D. Petrasso, R. P. J. Town, P. A. Amendt, S. P. Hatchett, O. L. Landen, A. J. Mackinnon, P. K. Patel, V. Smalyuk, J. P. Knauer, T. C. Sangster, and C. Stoeckl, Rev. Sci. Instrum. **77**, 10E725 (2006).

[18]J. R. Rygg, F. H. Séguin, C. K. Li, J. A. Frenje, M. J.-E. Manuel, R. D. Petrasso, R. Betti, J. A. Delettrez, O. V. Gotchev, J. P. Knauer, D. D. Meyerhofer, F. J. Marshall, C. Stoeckl, and W. Theobald, Science **319**, 1223 (2008).

[19]C. K. Li, F. H. Séguin, J. R. Rygg, J. A. Frenje, M. Manuel, R. D. Petrasso, R. Betti, J. Delettrez, J. P. Knauer, F. Marshall, D. D. Meyerhofer, D. Shvarts, V. A. Smalyuk, C. Stoeckl, O. L. Landen, R. P. J. Town, C. A. Back, and J. D. Kilkenny, Phys. Rev. Lett. **100**, 225001 (2008).

[20]Y. Lin, T. J. Kessler, and G. N. Lawrence, Opt. Lett. **20**, 764 (1995).

[21]T. R. Boehly, V. A. Smalyuk, D. D. Meyerhofer, J. P. Knauer, D. K. Bradley, R. S. Craxton, M. J. Guardalben, S. Skupsky, and T. J. Kessler, J. Appl. Phys. **85**, 3444 (1999).

[22]S. P. Regan, J. A. Marozas, R. S. Craxton, J. H. Kelly, W. R. Donaldson, P. A. Jaanimagi, D. Jacobs-Perkins, R. L. Keck, T. J. Kessler, D. D. Meyerhofer, T. C. Sangster, W. Seka, V. A. Smalyuk, S. Skupsky, and J. D. Zuegel, J. Opt. Soc. Am. B **22**, 998 (2005).

[23]S. Agostinelli, J. Allison, K. Amako, J. Apostolakis, H. Araujo, P. Arce, M. Asai, D. Axen, S. Banerjee, G. Barrand, F. Behner, L. Bellagamba, J. Boudreau, L. Broglia, A. Brunengo, H. Burkhardt, S. Chauvie, J. Chuma, R. Chytracek, G. Cooperman, G. Cosmo, P. Degtyarenko, A. Dell'Acqua, G. Depaola, D. Dietrich, R. Enami, A. Feliciello, C. Ferguson, H. Fesefeldt, G. Folger, F. Foppiano, A. Forti, S. Garelli, S. Giani, R. Giannitrapani, D. Gibin, J. J. Gómez Cadenas, I. González, G. Garcia Abril, G. Greeniaus, W. Greiner, V. Grichine, A. Grossheim, S. Guatelli, P. Gumplinger, R. Hamatsu, K. Hashimoto, H. Hasui, A. Heikkinen, A. Howard, V. Ivanchenko, A. Johnson, F. W. Jones, J. Kallenbach, N. Kanaya, M. Kawabata, Y. Kawabata, M. Kawaguti, S. Kelner, P. Kent, A. Kimura, T. Kodama, R. Kokoulin, M. Kossov, H. Kurashige, E. Lamanna, T. Lampén, V. Lara, V. Lefebure, F. Lei, M. Liendl, W. Lockman, F. Longo, S. Magni, M. Maire, E. Medernach, K. Minamimoto, P. Mora de Freitas, Y. Morita,

K. Murakami, M. Nagamatu, R. Nartallo, P. Nieminen, T. Nishimura, K. Ohtsubo, M. Okamura, S. O'Neale, Y. Oohata, K. Paech, J. Perl, A. Pfeiffer, M. G. Pia, F. Ranjard, A. Rybin, S. Sadilov, E. Di Salvo, G. Santin, T. Sasaki, N. Savvas, Y. Sawada, S. Scherer, S. Sei, V. Sirotenko, D. Smith, N. Starkov, H. Stoecker, J. Sulkimo, M. Takahata, S. Tanaka, E. Tcherniaev, E. Safai Tehrani, M. Tropeano, P. Truscott, H. Uno, L. Urban, P. Urban, M. Verderi, A. Walkden, W. Wander, H. Weber, J. P. Wellisch, T. Wenaus, D. C. Williams, D. Wright, T. Yamada, H. Yoshida, and D. Zschiesche, Nucl. Instrum. Methods Phys. Res. A **506**, 250 (2003).

[24] J. Delettrez, R. Epstein, M. C. Richardson, P. A. Jaanimagi, and B. L. Henke, Phys. Rev. A **36**, 3926 (1987).

[25] N. W. Jang, R. Betti, J. P. Knauer, O. Gotchev, and D. D. Meyerhofer, Bull. Am. Phys. Soc. **51**, 144 (2006).

[26] P. B. Radha, V. N. Goncharov, T. J. B. Collins, J. A. Delettrez, Y. Elbaz, V. Yu. Glebov, R. L. Keck, D. E. Keller, J. P. Knauer, J. A. Marozas, F. J. Marshall, P. W. McKenty, D. D. Meyerhofer, S. P. Regan, T. C. Sangster, D. Shvarts, S. Skupsky, Y. Srebro, R. P. J. Town, and C. Stoeckl, Phys. Plasmas **12**, 032702 (2005).